Final Draft
of the original manuscript:

Bystrzanowski, S.; Bartels, A.; Clemens, H.; Gerling, R.:
Characteristics of the tensile flow behavior of Ti–46Al–9Nb sheet material – Analysis of thermally activated processes of plastic deformation
In: Intermetallics (2008) Elsevier

DOI: 10.1016/j.intermet.2008.02.008

Characteristics of the tensile flow behavior of Ti-46Al-9Nb sheet-material - Analysis of thermally-activated processes of plastic deformation.

S. Bystrzanowski[a], *A. Bartels[a], H. Clemens[b], R. Gerling[c]

[a]Institute of Materials Science and Technology, Hamburg University of Technology, D-21071 Hamburg, Germany

[b]Department of Physical Metallurgy and Materials Testing, Montanuniversität Leoben, A-8700 Leoben, Austria

[c]Institute of Materials Research, GKSS-Research Centre, D-21502 Geesthacht, Germany

* corresponding Author

Abstract:

Flow behavior, strain hardening and activation parameters, i.e. activation volume, stress exponents and normalized free enthalpy of activation of Ti-46Al-9Nb sheet with near-gamma microstructure have been investigated in tension tests between 700 and 1000°C. The dependence of yield stress on temperature and strain rate, the course of the strain hardening curves and the values of activation parameters show that thermally-activated dislocation mechanisms are mainly involved in the tensile deformation process of the investigated material. At constant temperature the value of the activation volume depends both on plastic strain and strain rate. The activation volume generally decreases with increasing strain. The decrease is particularly well observable for higher strain rates, thus indicating a growing role of thermally-activated climb mechanisms governing the process of dynamic recovery. The activation volume calculated for a constant plastic strain (2% in case of this study) is a function of temperature and strain rate. At lower deformation rates, or alternatively at higher temperatures, the activation volume increases. Such behavior indicates a decrease in

dislocations density due to the onset of dynamic recrystallization. The analysis of stress exponents and the obtained free enthalpy of activation confirm that different thermally-activated processes are acting during deformation under the tensile test conditions studied.

Keywords:

Titanium aluminides, based on TiAl (A), mechanical properties at high temperatures (B), plastic deformation mechanisms (B), Work hardening (B), mechanical testing (F), texture (F)

1. Introduction:

High Nb containing γ-TiAl based alloys, TNB-alloys called for short, belong to the group of most promising light-weight structural materials for use at intermediate temperatures (~650 – 800°C) in aerospace and automotive applications. Due to high additions of Nb their tensile strength, creep strength as well as their oxidation resistance have been significantly improved, when compared to low Nb bearing TiAl alloys. Therefore, the TNB-alloys have been in focus of intensive studies aiming at an explanation of the role of large Nb additions on strengthening, phase transformations and microstructure control [1 - 5]. However, only little attention has been paid to plastic deformation of TNB-materials and to such aspects as strain hardening, dynamic recovery and/or dynamic recrystallization, i.e. processes which have a practical and important meaning in engineering applications [6]. Consequently, these topics will be treated in this study. The powder metallurgically processed Ti-46Al-9Nb (at%) sheet material is characterized with regard to its mechanical properties. Furthermore, the mechanisms occurring during tensile deformation will be discussed.

The aim of the present paper is to interpret the tensile flow behavior of Ti-46Al-9Nb sheets in the temperature range of 700 - 1000°C by means of thermal activation theory. This goal has been achieved through analysis of the general stress-strain and strain hardening behavior as

well as by determination and discussion of activation parameters, the apparent free enthalpy of activation and stress exponents.

2. Starting Ti-46Al-9Nb sheet material

The investigated sheet material was hot-rolled from compacts obtained by a powder metallurgical (PM) route. Alloy powder with chemical composition of Ti-46Al-9Nb (at%) was produced by means of plasma melting inert gas atomization [7] and subsequently hot-isostatically pressed to dense powder compacts. The compacts were then cross-rolled to sheets (dimensions: 600×300×1.2mm^3) at Plansee AG, Austria. After rolling, the sheets were subjected to primary annealing for 3 hours at 1000°C in order to flatten them and to minimize residual stresses. The result of this heat treatment is a primary annealed near gamma (PA/NG) microstructure which consists of areas of globular γ-TiAl grains with diameters in the range of 10 - 15 μm. These areas are surrounded by recrystallized regions consisting of small (~ 1 – 3 μm) γ-TiAl and α_2-Ti_3Al grains as shown in Fig. 1. Another feature of the starting microstructure is a large number of annealing twins. These twins were formed during primary annealing. Their presence indirectly indicates the low stacking fault energy of high Nb containing TiAl alloys [8].

3. Experimental

3.1 Tensile tests

Tensile specimens as shown in Fig. 2 were taken in rolling direction from the sheet with PA/NG microstructure. Two kinds of tensile experiments have been carried out. In the first case the tensile tests involved one sample for every temperature-strain rate condition. These

tests were carried out in the temperature range of 700 – 1000°C using 50°C-increments. The tests were performed until the specimen failed. For each temperature three different strain rates (between 1×10^{-6} 1/s and 1×10^{-3} 1/s, depending on test temperature) were applied. The experiments allowed us to characterize the general flow behavior of the material and to determine mechanical properties, i.e. 0.2% yield strength ($\sigma_{0.2}$), ultimate tensile strength (σ_m), saturation stress (σ_s), and fracture strain. Additionally, the obtained data were used to calculate the stress exponents and the apparent activation energies in the steady state condition.

The second type of experiment involved strain rate jump tests: The initial deformation rate was increased by a factor of 3 and kept constant within an elongation step of $\Delta\varepsilon = 0.01$. At the end of this elongation step the deformation rate was decreased to the initial value and kept constant for another $\Delta\varepsilon = 0.01$. These steps were cyclically repeated while the temperature (750, 825 and 900°C) was kept constant. For each temperature up to 10 strain rate jumps at different strains were used for the evaluation of the strain rate sensitivity and the activation volume.

The experiments were performed using a tensile test machine Zwick 1474. In order to control the test temperature accurately, a three-zone pipe furnace supplied with a three-zone heat controller device has been used. The temperature was measured directly on the specimen by means of two thermocouples (Pt/Rh-Pt, type-S) located at opposite ends of the sample.

All tensile tests in the present study were conducted in air. In order to ensure a constant strain rate, the speed of the cross-head was regulated by a controlling program, which calculates the actual elongation corrected by the elastic modulus of both, sample and test machine. Then, on basis of true plastic elongation, the exact velocity of the traverse required to keep the strain rate constant, is calculated.

Immediately after failure of the sample the furnace was opened and the specimen was rapidly cooled to room temperature by pressurized air. This procedure allowed us to ″freeze″ the deformation microstructure and texture.

3.2 Texture measurements

For the measurement of the initial sheet texture a sample with dimensions of 20×21 mm^2 was used. After surface preparation (grinding and polishing) the specimen was subjected to the texture measurement, which was performed by means of X-ray diffraction. A new parallel beam geometry technique, which offers the possibility to measure pole figures up to an inclination angle of 85°, was employed [9]. Among with the strong {111} reflection, also the relatively weak superlattice reflections (001), {110} and {201} were used in this study. On the basis of the four measured pole figures the orientation distribution function (ODF) has been calculated by employing the harmonics method [10].

4. Results and discussion

4.1 Texture of the starting Ti-46Al-9Nb sheet material

Fig. 3 exhibits a result of texture measurements conducted on the starting sheet used for the tensile experiments throughout this study. The result is presented in form of the well known stereographic projection as recalculated (001)-pole figure. The texture is very weak and no distinct orientation maxima can be recognized. Only weak maxima can be seen around the transversal direction of the sheet, which correspond to the modified cube texture component. This cube texture is caused by recrystallization during reheating between individual passes of

the rolling process and by the subsequent primary annealing treatment [9]. The four maxima near the center of the pole figure indicate an ideal twin orientation with regard to the modified cube component [7, 11]. The sheets of the present study were cross-rolled, which in our particular case means that the second and fourth rolling passes have been conducted in transverse direction (TD) to the original rolling direction (RD) of the sheet. Consequently, the modified cube texture is much weaker than in a sheet rolled in one direction only, as reported for the same material in ref. [7]. Tensile tests conducted on samples prepared parallel and perpendicular to the rolling direction of sheets which were exclusively rolled in one direction showed an isotropic deformation behavior between 700 and 1000°C [7]. Therefore, due to the weak texture of the investigated cross-rolled sheets we did not expect any mechanical anisotropy. Thus, all tensile tests were performed in the direction of the final rolling steps. More information about textures in powder metallurgically processed γ-TiAl based sheets of different compositions can be found in [9, 12-14].

4.2 General flow stress and strain hardening behavior

The flow stress and strain hardening behavior of Ti-46Al-9Nb sheet as a function of temperature and strain rate is shown in Figs. 4 and 5. In Fig. 4a the true tensile stress versus true strain for different temperatures between 750 and 1000°C is plotted for a constant strain rate of 1×10^{-4} 1/s. The shapes of the curves indicate a strong dependence of the flow behavior on temperature. At 750°C the material was hardly deformable in uniaxial tension and failed at a true plastic strain of only ~ 0.05. An increase in test temperature to 800°C increases the plasticity of the material dramatically leading to a true fracture strain of ~ 0.42. The significant increase in ductility as observed at 800°C occurs as a result of the growing role of softening processes, such as dynamic recovery (DR) due to an increased dislocation mobility and/or dynamic recrystallization (DRX), while the latter process has a larger contribution at

higher temperatures. For example, in Fig. 4a the presence of DRX is especially well manifested in the tensile curves obtained at 900, 950 and 1000°C. These curves show a maximum of the flow stress around $\varepsilon \leq 0.04$, followed by a monotonic and nearly linear decrease of the stress with increasing strain. At higher strains a plateau in the stress/strain curve is expected [15]. However, as a consequence of necking the onset is not visible in our case.

From Fig. 4b it is discernible that for a constant temperature the flow stress is strongly dependent on strain rate. Fig. 4c summarizes the temperature dependence of yield stress ($\sigma_{0.2}$) and ultimate tensile strength (σ_m) for a constant strain rate of 1×10^{-4} 1/s. It should be noted that σ_m has been determined on the basis of the true stress true strain diagrams in Fig. 4a, i.e. it represents a true stress value referring to the actual mean cross section of the specimen. Fig. 4c shows a continuous decrease of the flow stress level with increasing temperature. This is due to enhanced thermally-assisted overcoming of obstacles by mobile dislocations [16]. With increasing temperature the thermal component (σ^*) and, consequently, the total flow stress (σ) of the material which consists of two contributions: $\sigma = \sigma_\mu + \sigma^*$, is decreased. The component σ_μ represents the athermal part of the total flow stress which is almost independent on temperature (only by the temperature dependence of the shear modulus μ). Furthermore, the dependence of $\sigma_{0.2}$ on temperature can be subdivided in three ranges. Firstly, at temperatures below 800°C the curve shown in Fig. 4c exhibits a flat course (first range) turning into a steeper slope between temperatures of 800 and 950°C (second range). In this temperature range an almost exact linear dependence of $\sigma_{0.2}$ on temperature is observed. It can be described by $\sigma_{0.2}/\text{MPa} = 1762 - 1.65\times T/°C$. Finally, at temperatures above 950°C the slope of the $\sigma_{0.2}$ curve is slightly decreased again (third range). It is noteworthy, that a similar trend has been observed for Ti-47at.%Al-2at.%Mn-2at.%Nb-0.8vol.%TiB_2 with nearly lamellar microstructure [17].

The strain hardening behavior of the Ti-46Al-9Nb sheet can be analyzed using so-called Θ vs. σ plots, where Θ is the strain hardening coefficient, defined as $\Theta = d\sigma/d\varepsilon$; σ and ε are the true stress and the true strain, respectively [18-20].

The Θ-σ plots represent the so-called third stage of strain hardening which is characterized by the competition of deformation-induced hardening and thermally-assisted softening of the material, occurring as a result of DR and/or DRX [19]. The hardening rate is strongly dependent on temperature and strain rate as can be deduced from Figs. 5a and b.

At constant strain rate and lower temperatures (e.g., at 1×10^{-4} 1/s and 750 – 800°C, see Fig. 5a) as well as at constant temperature and higher strain rates (e.g. at 850°C and 3×10^{-4} 1/s, 1×10^{-3} 1/s, see Fig. 5b) the Θ-curves exhibit a pronounced change in the slope. Initially, the rate of the decrease of Θ with increasing flow stress is quite high. This is reflected in the initial steep branch of the curves. At higher stresses the course of the hardening rate is characterized by a decreased slope. In contrast, at higher temperatures, i.e. > 850°C, only a rapid straight decrease of Θ can be observed (Fig. 5a). This regime is frequently interpreted in terms of Voce's stress/strain dependence [16, 19]. It has already been pointed out by Kocks and Mecking [19] that the Voce's law gives a good approximation for some regimes of the strain hardening, but it does not fit the entire stress-strain curve. This observation is also confirmed in our case, as deduced from the course of the strain hardening curves shown in Fig. 5. A deviation from linearity in the Θ-curves can generally be observed at higher stresses / strain rates.

The different behavior of the strain hardening curves may be caused by a change in the mechanisms which control the dislocation processes. For example, it is commonly accepted in literature that the thermally-activated processes of re-arrangement of dislocations (dynamic recovery), which basically govern the strain hardening behavior of the third stage, are controlled by cross slip at lower temperatures, while at higher temperatures dislocation climb

becomes the predominant mechanism [15, 21]. Moreover, at very high temperatures, in our case in the range of 900 – 1000°C, the hardening rate is additionally affected by the onset of dynamic recrystallization processes, which consequently give a contribution to the drastic decrease of Θ. Apart from recovery processes, an other mechanism which also contributes to an overall diminishing of the strain hardening rate of the material during the third stage might be a group movement of dislocations, localized in slip (or shear) bands.

Θ versus σ plots shown in Fig. 5 have subsequently been used for the estimation of the saturation or steady state stress (σ_s). The saturation stress corresponds to the equilibrium between athermal hardening and thermally-activated softening processes. In the ideal case it is equivalent to the hardening coefficient $\Theta = d\sigma/d\varepsilon \rightarrow 0$. However, due to necking σ_s cannot experimentally be proven in a tensile test. Therefore, for the determination of σ_s the last linear sections of the Θ-σ curves have been extrapolated to $\Theta \rightarrow 0$ (see Fig. 5). All calculated σ_s values are summarized in Table 1. Subsequently, the values of the saturation stress have been used for the determination of stress exponents as well as for the evaluation of activation energies of thermally-activated recovery processes in the steady-state condition.

4.3 Activation volume and strain rate sensitivity

By means of strain rate jump experiments the thermally-activated processes of dislocation slip have been investigated at 750°C, 825°C and 900°C. Throughout these experiments the strain rate sensitivity has been analyzed and the activation volume was calculated according to [22]:

$$V = \frac{f\, k_B T}{\left.\frac{\Delta\sigma}{\Delta \ln \dot{\varepsilon}}\right|_{T=const}} \qquad (1)$$

where V is an activation volume, f represents the Taylor factor (here f = 3.06) and k_B the Boltzmann constant.

The activation volume is a parameter which is commonly used to characterize the interaction mechanisms of mobile dislocations with short-range obstacles during the process of plastic deformation. The value of the activation volume, which can be expressed according to: $V = bdl$ (b: Burgers vector, b = 0.283 nm for TiAl; d: diameter of the obstacle, also called an activation distance; l: distance between the obstacles), indicates the character of the obstacles, i.e. their size and/or their distribution in the material. Consequently, the value of V, commonly expressed in units of b^3, indicates whether or not an obstacle can be surmounted by means of thermal fluctuations. It is known that only short-range obstacles, which are associated with $V = 1 - 10\ b^3$, might be overcome by means of thermal activation [23]. In the following our analysis is solely restricted to possible interactions between mobile dislocations and short-range obstacles, represented by forest dislocations. There is of course an awareness that such assumption made for a two-phase material like Ti-46Al-9Nb is not without criticism. In particular, the dislocation mobility can be affected by the presence of the second phase and its distribution, but also by the concentration of impurities, possible phase transformations as well as new phases which might be formed during deformation, etc.. All these factors make the analysis of the deformation process much more complex and affect the activation volume. However, for simplicity the changes of the activation volume will be analyzed as a function of only one variable, i.e. the density of the immobile (forest) dislocations.

Fig. 6 shows representative stress-strain curves obtained during strain rate jump tests conducted at two distinct temperatures of 750 and 900°C. On the basis of such curves the strain rate sensitivity of the material has been analyzed. The strain rate sensitivity is defined as:

$$S = \frac{d\sigma}{d \ln \dot{\varepsilon}} \cong \frac{\Delta\sigma}{\Delta \ln \dot{\varepsilon}}, \qquad (2)$$

and it characterizes the response of the stress to a strain rate jump. The stress increment ($\Delta\sigma$)

which occurs directly after the strain rate jump has been estimated by means of extrapolation as indicated in Fig. 6. For both temperatures a similar strain rate sensitivity behavior can be observed. A sudden increase in strain rate leads to an immediate increase in stress. However, the course of the stress-strain curve presented in Fig. 6b indicates that at a test temperature of 900°C the material already suffers from structural changes which are reflected in the continuous decrease of the stress level for the duration of the deformation process. Such behavior is not observed at 750°C, where the flow stress increases continuously. The structural changes at 900°C result from a dominant role of the softening processes (DR and probably DRX). It can be assumed that softening generally increases with decreasing strain rate and increasing temperature and strain. Due to the response of stress to changes of $\dot{\varepsilon}$ the calculated activation volumes are influenced by the occurring softening phenomena as well [1].

In order to minimize the influence of these processes the corresponding activation volumes have been evaluated at the beginning of plastic deformation, i.e. at a small plastic strain of $\varepsilon = 0.02$. It is assumed that during such a small predeformation no significant change of the microstructure occurs. Moreover, it can be taken into account that at a small elongation of $\varepsilon \sim 0.02$, caused by a relatively low flow stress, ordinary dislocations should be activated initially. The latter assumption is corroborated by the fact that the critical resolved shear stress (CRSS) for activation of ordinary dislocations in TiAl is much lower than the CRSS for activation of superdislocations and twinning [24-26]. Consequently, the V values estimated at $\varepsilon \sim 0.02$ should mainly characterize a pure dislocation-dislocation interaction on the slip plane. Furthermore, at 825°C and 900°C additional experiments were conducted using a higher initial strain rate, i.e. 1×10^{-4} 1/s. As a consequence, both the onset of DR and DRX is shifted to higher strains.

In the following, the changes of the activation volume as a function of strain are described. The influence of all parameters, i.e. temperature, strain rate and strain, on the activation volume is summarized in Figs. 7a and b.

From Fig. 7a it can be seen, that the activation volume is strongly strain dependent. At 750°C and for an initial strain rate of 1×10^{-5} 1/s the reciprocal activation volume shows a linear increase with strain. Applying the same initial strain rate at a temperature of 825°C results in similar strain dependence of 1/V, but the slope is reduced when compared to 750°C. Furthermore, at a temperature of 900°C and an initial strain rate of 1×10^{-5} 1/s 1/V decreases significantly as strain increases, which might be an indication for the growing role of softening/recrystallization processes. It is interesting to note that at a temperature of 825°C an increase of the initial strain rate by a factor of 10 (from 1×10^{-5} 1/s to 1×10^{-4} 1/s) leads to a significant increase in the slope of the 1/V curve (Fig. 7a). This phenomenon can be explained in terms of the Orowan equation which correlates strain rate and dislocation density:

$$\dot{\varepsilon} = \rho_m b\, v \cong \rho_m b\, l\, \nu_D \exp\left(-\frac{\Delta G}{k_B T}\right) \qquad (3)$$

The parameters in equation (3) have the following meanings: ρ_m: density of mobile dislocations; v: average dislocation velocity; l: slip path after successful activation; ν_D: Debye frequency; ΔG: free energy of activation, i.e. the energy that must be supplied by thermal fluctuations at constant temperature and stress [27]. Assuming that at a constant temperature the activation energy is constant and depends only weakly on stress, a sudden increase of the strain rate, e.g. by a factor of 10 must lead to a significant increase of the dislocation density. Consequently, the number of mutual interactions increases too. In addition, the number of point defects will be increased. Therefore, it is tempting to speculate that the increased density of defects will lead to an enhancement of the climb processes at elevated temperatures [23]. This suggestion is confirmed by a strong increase of the reciprocal activation volume with

strain. Such behavior indicates a growing role of thermally-activated processes on dislocation climb.

The same test procedure has been applied at 900°C (Fig. 7a). In this case a very strong increase of 1/V with increasing strain is observed up to $\varepsilon \cong 0.05$. Above this strain level the curve show a rather flat branch. This means that the same softening mechanisms, which occur at 900°C and an initial strain rate of 1×10^{-5} 1/s already at the beginning of deformation, become active/dominant after several percent of deformation at the same temperature when an initial strain rate of 1×10^{-4} 1/s is applied.

Fig. 7b briefly summarizes the influence of temperature and strain rate on the activation volume which has been estimated at an elongation of $\varepsilon \approx 0.02$. It can be seen that an increase of temperature generally leads to an increase of the reciprocal activation volume which corresponds to a decrease of the V value. For example, the activation volume determined at the initial strain rate of 1×10^{-5} 1/s decreases between 750°C and 825°C from $V = 42b^3$ to $V = 34b^3$. At 900°C, however, it increases again to $V = 46b^3$. A larger V suggests that the obstacle (forest dislocation) distance has increased as a result of a diminished density of dislocations due to onset of DRX. Such behavior has not been observed during the test at a higher initial strain rate, i.e. 1×10^{-4} 1/s. Here, the activation volume calculated for $\varepsilon \approx 0.02$ decreases from $V = 42b^3$ at 825°C to $V = 35b^3$ at 900°C.

It should be noted that our values of the activation volume are of similar order of magnitude as those reported by Appel et al. [23] for other high Nb containing TiAl alloys. Some exemplary data are plotted in Fig. 7b for comparison. An exact matching of all data is not expected since the alloys differ with respect to chemical composition, processing history, microstructure, and test conditions.

The activation volumes for Ti-46Al-9Nb as shown in Fig.7b vary between $34b^3$ and $46b^3$. These values are higher than those theoretically predicted for dislocation climb ($1b^3$ - $10b^3$).

According to Appel et al. [23] such a discrepancy may originate from superposition of dislocation climb with other processes on atomic scale. Furthermore, a higher value of the activation volume might be a result of widely separated (super) dislocations. It should be emphasized that such dislocation configurations occur easily in TNB-alloys as a result of the lowered stacking fault energy due to high Nb additions [1, 8, 28, 29].

4.4 Stress exponents and activation energies

The stress exponents n have been calculated from the $\dot{\varepsilon}$ vs. σ_s/μ diagram shown in Fig. 8a. The σ_s data are summarized in Table 1. The temperature dependence of the shear modulus of Ti-46Al-9Nb was estimated from the elastic modulus data reported in [30]. It can be seen from Fig. 8a that the stress exponent decreases with increasing temperature, or alternatively, with decreasing stress. The experimental error in ln σ_s/μ results from the linear extrapolation for the determination of σ_s (Fig. 5). The error ranges around the size of the symbols and, therefore, is not shown in Fig. 8a. The n-value varies from 9.4 at 700°C and high stresses to 3.8 at 1000°C and low stress levels. The obtained values are in good agreement with those found for pure metals, i.e. $4 \leq n \leq 8$, in which the lower value is usually observed at higher temperatures [15]. A possible reason for this phenomenon can be a change of the prevailing deformation mechanism, i.e. processes predominating at low temperatures (and higher stresses), e.g. cross slip, are replaced by processes prevailing at high temperatures (and lower stresses), e.g. dislocation climb [15].

Fig. 8b shows the strain rate vs. normalized saturation stress or steady-state stress in a double logarithmic plot as obtained from short-term tensile tests as well as creep tests. Both types of tests were conducted at a temperature of 700°C. Since an equivalency of tensile and creep tests has been confirmed for steady-state conditions [15], a direct comparison of data derived from these two different tests is allowed. The compiled data in Fig. 8b indicate clearly a

typical "power law break-down" behavior. At higher stresses a high n-value of 9.4 is prevailing, while n decreases to 4.2 at lower stresses. A high n-value is frequently interpreted as larger contributions of dislocation glide to the combined dislocation glide and climb mechanisms [31]. It should be noted that a power law break-down behavior in TiAl alloys has also been reported by other authors [31, 32].

Thermally-activated dislocation processes can be described by the temperature and stress dependent free enthalpy of activation $\Delta G(\sigma, T)$ [16]. In order to take into account entropy effects due to the temperature dependence of the elastic constants a scaled temperature variable ($\mu b^3/kT$) is introduced. Consequently, the measured activation enthalpy ΔG must be normalized to μb^3 [27]. This gives a correction for the temperature dependences and thus makes the conversion of activation enthalpy (ΔH) into free activation enthalpy (ΔG) not necessary [16, 27].

To determine $\Delta G/\mu b^3$ the strain rates evaluated from the data in Fig. 8a at six constant values of $\ln \sigma_s/\mu$ (-4.5, -4.7,-4.9, -5.1, -5.3, -5.5. Indicated as dashed lines in Fig. 8a) are plotted in Fig. 9a in form of an Arrhenius plot using the scaled temperature variable ($\mu b^3/kT$). It is evident that not all data points in Fig. 9a are laying on straight lines exactly, especially in the range of higher temperatures (see data connected with dotted lines in Fig. 9a). This means, that the free enthalpy of activation ($\Delta G/\mu b^3$) is not constant in the temperature/stress range investigated. Therefore, the determination of $\Delta G/\mu b^3$ was restricted to the range of strain rates connected with solid lines in Fig. 9a, which is closest to the strain rates used in the experiments.

The $\Delta G/\mu b^3$ values plotted against the normalized saturation stress $\sigma_s/\mu b^3$ exhibit a "U"-like course as shown in Fig. 9b. The error bars in Fig. 9b reflect the uncertainty in $\Delta G/\mu b^3$ due to the experimental errors in σ_s. For higher stresses (and temperatures between 700 and 900°C) the curve develops a flatter branch, while $\Delta G/\mu b^3$ reaches values around 0.38. This part

describes most probably thermally-assisted recovery processes by dislocation climb. Then, the value of $\Delta G/\mu b^3$ drops to about 0.32. This value has been determined at intermediate stresses and temperatures between 850 and 1000°C. Such behavior indicates that another, thermally-activated process with lower activation enthalpy becomes significant and influences the flow kinetics. The observed decrease of the activation energy might be assigned to phase transformation processes which occur during creep testing at a temperature around 850°C. These structural processes have been investigated by means of SEM and X-ray examinations [33]. As a result of these processes the α_2-phase transforms into very fine-grained ω-phase. These fine-grained ω zones may act as the "lubricant" for larger grains and, thus, facilitating plastic flow which is reflected in the reduced value of the activation energy.

Finally, at low stresses and temperatures between 900 and 1000°C the activation enthalpy increases again, which points at another thermally-controlled process. Probably, the increasing activation enthalpy reflects the onset of DRX processes. This assumption is in agreement with observations that DRX in TiAl alloys is characterized by a high activation energy (~ 400 kJ/mol) combined with an n-value around 5 [15, 34].

5. Summary

In this study the general tensile flow behavior, the strain hardening characteristics as well as thermally-activated processes of Ti-46Al-9Nb sheet material have been characterized in the temperature range of 700 – 1000°C and the results can be summarized as follows:

- At elevated temperatures, this ordered intermetallic alloy behaves to some extend like conventional bcc or fcc metals. This concerns especially the stress/strain characteristic, the strain hardening and the related "Voce law" behavior and the stress exponents.

- Flow behavior and ductility show a strong dependence on temperature and strain rate. At a constant strain rate of 1×10^{-4} 1/s a drastic increase in plasticity with increasing temperature is observed above 800°C.
- Between 850 and 950°C the yield stress decreases linearly with temperature at constant strain rates.
- During straining the strain hardening rate Θ always drops rapidly from high initial values down to about 2000 MPa and subsequently decreases linearly until the saturation stress σ_s is reached. With increasing temperatures or with lower applied strain rates the linear decrease of the strain hardening rate becomes steeper.
- At temperatures ≥900°C the decrease of the strain hardening rate becomes as fast as the initial decrease.
- The activation volume V calculated at constant strain ($\varepsilon = 2\%$) decreases with increasing temperature from $V = 42b^3$ at 750°C to $V = 34b^3$ at 825°C. This indicates a growing role of thermally-activated climb processes. The increase at 900°C up to $V = 46b^3$ might be attributed to the onset of dynamic recrystallization which leads to a decrease of the dislocation density.
- At lower test temperatures and at higher strain rates the activation volume decreases as the plastic strain increases. Such behavior indicates the growing role of dislocation interaction, i.e. the mean free path of mobile dislocations is reduced by cutting processes as plastic deformation proceeds.
- The stress exponents are between 3.8 and 9.4, depending on the test conditions. Most values are in the typical range as frequently observed for other γ-TiAl based alloys ($n \leq 8$).
- A "U-like" profile of the apparent activation enthalpy is found in the investigated stress regime, indicating the presence of three different thermally-controlled processes

which can be described as follows: Dynamic recovery at higher stresses and lower temperatures. Phase transformations and formation of fine-grained ω-phase at intermediate stresses and temperatures. Finally, onset of dynamic recrystallization which generally occurs at lower stresses and high temperatures.

6. Acknowledgement:

The financial support within the framework of the "Hochschulprogramm" of the GKSS Research Centre Geesthacht and by the Helmholtz Gesellschaft as "Virtuelles Institut für Werkstoffe des Leichtbaus" is gratefully acknowledged. Thanks go to Plansee AG, Austria, for sheet rolling.

7. References:

[1] Appel F, Wagner R. Mater Sci Eng 1998; R22: 187.

[2] Zhang WJ, Deevi SC, Chen GL. Intermetallics 2002; 10: 403.

[3] Zhang WJ, Appel F. Mater Sci Eng 2002; A329-331: 649.

[4] Zhang D, Dehm G, Clemens H. Z. Metallkde.; 91; 2000; 11: 950.

[5] Hu D. In: Lütjering G, Albrecht J. editors. Ti-2003 Science and Technology. Viley-VCH, Weinheim, Germany 2004; Vol.4: p. 2369.

[6] Paul JDH, Appel F. Metall. Mater. Trans. A; 2003; 34A: 2103.

[7] Gerling R, Bartels A, Clemens H, Kestler H, Schimansky F-P. Intermetallics 2004; 12: 275.

[8] Chen GL, Zhang WJ, Liu ZC, Li SJ. In: Kim Y-W, Dimiduk DM, Loretto MH editors. Gamma titanium aluminides. Warrendale, USA: TMS, 1999. p. 371.

[9] Schillinger W, Bartels A, Gerling R, Schimansky F-P, Clemens H. Intermetallics 2006; 14: 336

[10] Dahms M, Bunge HJ,. Textures and Microstructures 1998; 10: 97.

[11] Bystrzanowski S, Bartels S, Clemens H, Gerling R, Schimansky F-P, Dehm G, Kestler H. Intermetalics 2005; 13: 515.

[12] Bystrzanowski S, Bartels A, Clemens H, Gerling R, Schimansky F-P, Kestler H, Dehm G, Weller M. In: Lütjering G, Albrecht J editor. Ti-2003 Science and Technology. Viley-VCH, Weinheim, Germany 2004; Vol.4: p. 2401.

[13] Bartels A, Schillinger W, Graßl G, Clemens H. In: Kim Y-W,Clemens H, Rosenberger AH, editors. Gamma titanium aluminides. Warrendale, USA: TMS, 2003: p. 275.

[14] Bartels A, Hartig Ch, Willems S, Uhlenmut H. Mater Sci Eng 1997; A239-240: 14.

[15] Mecking H, Gottstein G. In: Haessner F editor. Recrystallization of Metallic Materials. Riederer Verlag, Stuttgart, Germany 1978: 195.

[16] Mecking H, Nicklas B, Zarubova N, Kocks UF. Acta metal. 1986; Vol.34; No.3: 527.

[17] Lin D, Wang Y, Law CC. Mater Sci Eng 1997;A239-240: 369.

[18] Mecking H. In: Thompson AW editor. Work Hardening in Tension and Fatigue. TMS AIME, New York, 1977: 67.

[19] Kocks UF, Mecking H. Progress in Mater Sci 2003;48: 171.

[20] Mecking H. In: Gundlach C, Haldrup K, Hansen N, Huang X, Jensen DJ, Leffers T, Li ZJ, Nielsen SF, Pantleon W, Wert JA, Winther G editors. Evolution of Deformation Microstructures in 3D. Riso National Laboratory, Roskilde, Denmark 2004: 431

[21] Mecking H. In: Haasen P, Gerold V, Kostorz G editors. Strength of Metals and Alloys. Pergamon Press. Toronto, Oxford, New York, Sydney, Paris, Frankfurt. ICSMA 5; Vol.3; 1980: 1573.

[22] Schöck G. Phys. Stat. Solidi 1965; 8: 499.

[23] Appel F, Oehring M, Wagner R. Intermetallics 2000; 8: 1283.

[24] Bartels A, Hartig Ch, Willems S, Uhlenhut H. Mater Sci Eng 1997; A239-240:14.

[25] Bartels A, Kestler H, Clemens H. Mater Sci Eng 2002; A329-331: 153

[26] Schillinger W, Lorenzen B, Bartels A. Mater Sci Eng 2002; A329-331: 644

[27] Kocks UF, Argon AS, Ashby MF. Progress in Mater Sci; Pergamon Press.; Oxford, New York, Toronto Sydney, Braunschweig; 1975

[28] Zhang W-J, Appel F. Mater Sci Eng 2002; A329-331: 649.

[29] Appel F. Mater Sci Eng 2001; A317: 115.

[30] Weller M, Clemens H, Haneczok G, Dehm G, Bartels A, Bystrzanowski S, Gerling R, Arzt E. Phil. Mag. Letters 2004; Vol. 84; No.6: 383.

[31] Beddoes J, Triantafillou, Zhao L. In: Koch CC, Liu CT, Stoloff NS, Wanner A editors. High-Temperature Ordered Intermetallic Alloys VII. Mater Res Soc Proc; Vol. 460; Pittsburg (PA); MRS; 1997: 293.

[32] Nieh TG, Wang JN. Scripta Met Mater; 33; 1995; 1101

[33] Bystrzanowski S, Bartels A, Clemens H, Gerling R, Schimansky F-P, Dehm G. In: Mills M J, Inui H, Clemens H, Fu C-L. Integrative and Interdisciplinary Aspects of Intermetallics. Mater Res Soc Proc; Vol. 842; Warrendale (PA); MRS; 2005: 121

[34] Bartels A, Seeger J, Mecking H. In: I. Baker, R. Darolia, J.D. Whittenberger, M.H. Yoo editors. High-Temperature Ordered Intermetallic Alloys V. Mat. Res. Soc. Proc.; Vol.288; Pittsburg (PA); MRS, 1993: 1179.

Figure Captions

Figure 1:

Primary annealed near gamma microstructure of the Ti-46Al-9Nb sheet after annealing for 3 hrs at 1000°C. Scanning electron microscope image taken in back-scattered electron mode; dark to grey phase: γ-TiAl, bright phase: α_2-Ti_3Al. Note the presence of annealing twins (arrowed). The direction of rolling is vertical.

Figure 2:

Shape and dimensions in mm of the tensile specimens used in this study.

Figure 3:

Recalculated (001)-pole figure of the texture in cross-rolled Ti-46Al-9Nb sheet material. Ideal positions for the modified cube (closed symbols) and their related twin (open symbols) components are shown.

Figure 4:

Tensile flow behavior of Ti-46Al-9Nb sheet material: (a) true stress vs. strain curves for a constant strain rate of 1×10^{-4} 1/s and different temperatures; (b) representative true stress vs. strain curves for a constant temperature of 850°C and different strain rates; (c) temperature dependence of yield stress ($\sigma_{0.2}$) and ultimate tensile strength (σ_m) as derived from Fig. 4a. The evaluation of the depicted tensile tests is summarized in Table 1.

Figure. 5:

Θ-σ curves corresponding to the stress - strain curves of Figs. 4a and b: (a) different temperatures and constant strain rate (1×10^{-4} 1/s); (b) different strain rates and constant

temperature (850°C). Extrapolation of the linear part of the curves to $\Theta = d\sigma/d\varepsilon \rightarrow 0$ allows the determination of the saturation stress σ_s.

Figure. 6:

Representative stress-strain curves from strain rate jumps experiments performed at (a) 750°C and (b) 900°C. The starting strain rate is 1×10^{-5} 1/s and the strain rate increase is by a factor of 3. The determination of the stress increment $\Delta\sigma$ is indicated.

Figure. 7:

Deformation behavior of Ti-46Al-9Nb analyzed by means of the reciprocal activation volume: (a) dependence of the reciprocal activation volume 1/V on strain for two different initial strain rates and three different temperatures; (b) 1/V as a function of temperature as calculated for $\varepsilon = 0.02$ and two different strain rates. For comparison the activation volume of other TNB-alloys are indicated [1, 23].

Figure. 8:

(a) Strain rate vs. normalized saturation stress. The determined stress exponents are given in the inset. (b) Change of stress exponent at 700°C as a function of normalized saturation stress (tensile test) or steady-state stress (creep test).

Figure. 9:

(a) Arrhenius plots of the strain rates as obtained for constant values of σ_s/μ at different temperatures; (b) normalized free enthalpy of activation as a function of σ_s/μ.

Table 1: Mechanical properties of Ti-46Al-9Nb sheet material as obtained from tensile tests. $\sigma_{0.2}$: yield strength; σ_m: ultimate tensile strength; σ_s: saturation stress; ε_f: true fracture strain.

Temperature [°C]	Strain rate [1/s]	$\sigma_{0.2}$ [MPa]	σ_m [MPa]	σ_s [MPa]	ε_f
700	1×10^{-6}	419	535	536	0.18
	3×10^{-6}	462	-	588	0.12
	1×10^{-5}	508	-	682	0.07
750	1×10^{-5}	413	521	513	0.42
	3×10^{-5}	465	-	581	0.15
	1×10^{-4}	497	-	663	0.05
800	3×10^{-5}	381	455	451	0.46
	1×10^{-4}	440	546	532	0.42
	1×10^{-3}	520	-	702	0.04
850	1×10^{-4}	362	414	414	0.46
	3×10^{-4}	414	494	487	0.55
	1×10^{-3}	473	611	588	0.45
900	1×10^{-4}	278	304	304	0.51
	3×10^{-4}	343	370	370	0.47
	1×10^{-3}	403	458	454	0.49
950	1×10^{-4}	193	217	217	0.48
	3×10^{-4}	253	276	276	0.52
	1×10^{-3}	325	353	358	0.47
1000	1×10^{-4}	123	146	146	0.65
	3×10^{-4}	152	198	201	0.45
	1×10^{-3}	191	265	267	0.63

Figures

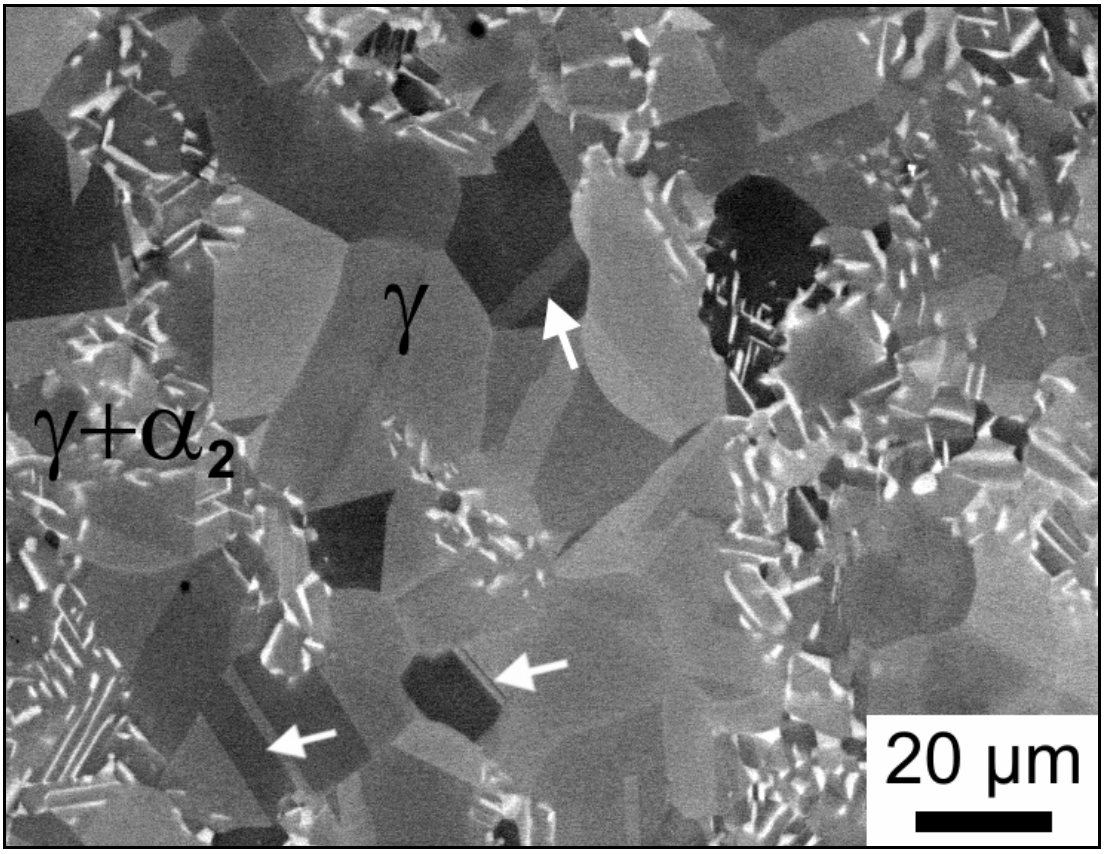

Figure 1

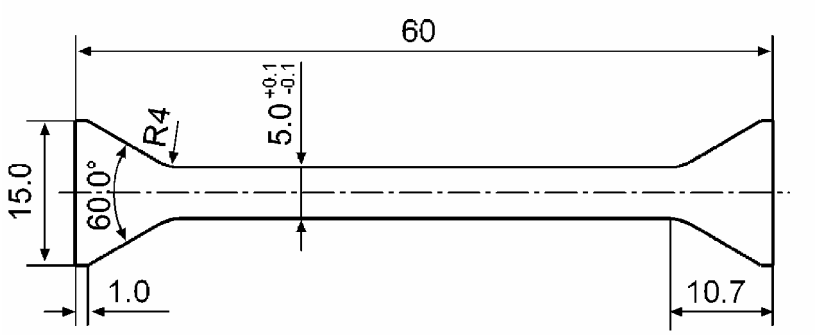

Figure 2

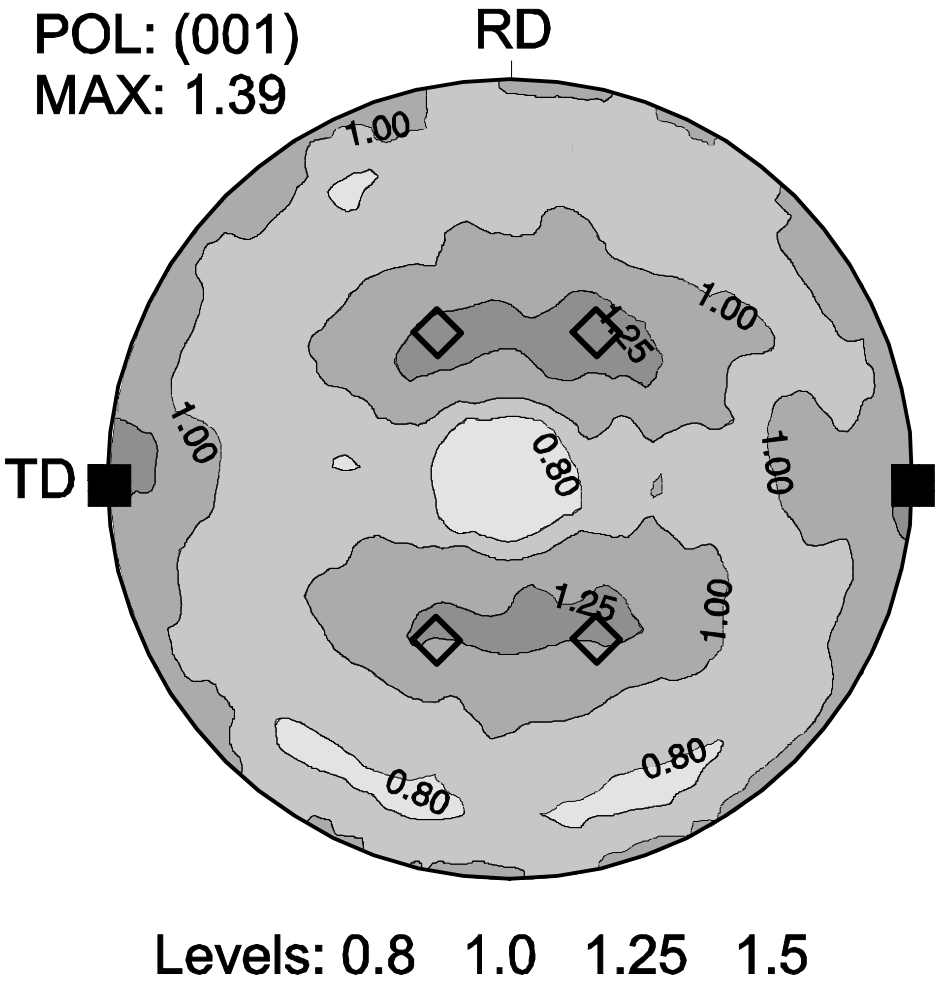
POL: (001)
MAX: 1.39
RD
TD
1.00
1.00
1.25
1.00
0.80
1.00
1.25
1.00
0.80
0.80
Levels: 0.8 1.0 1.25 1.5

Figure 3

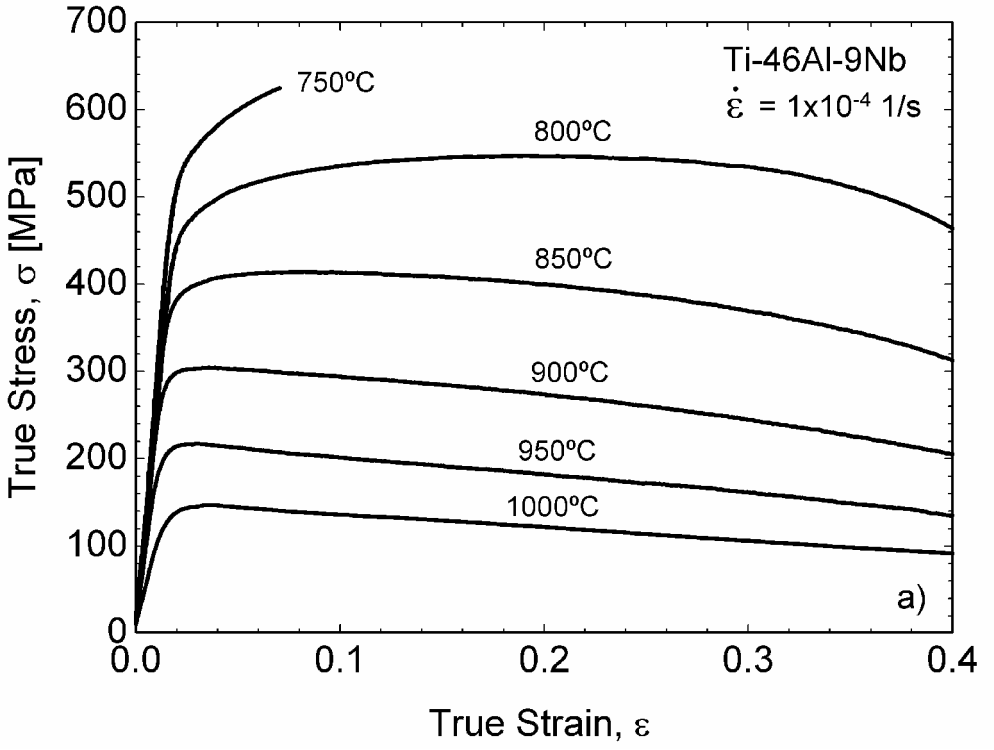

Figure 4a

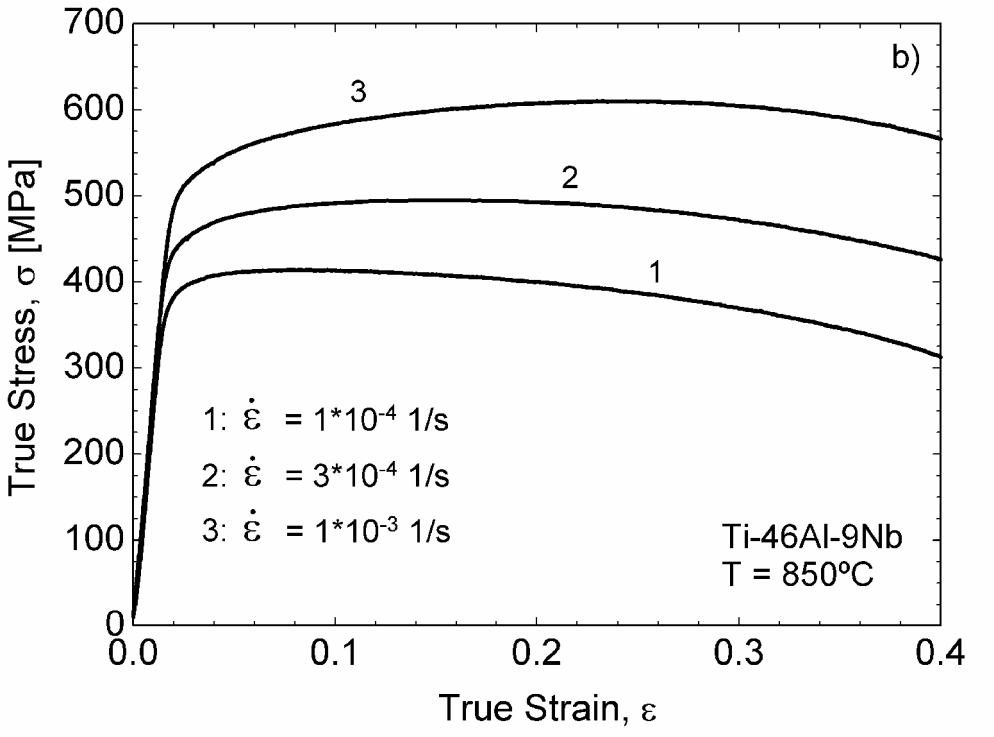

Figure 4b

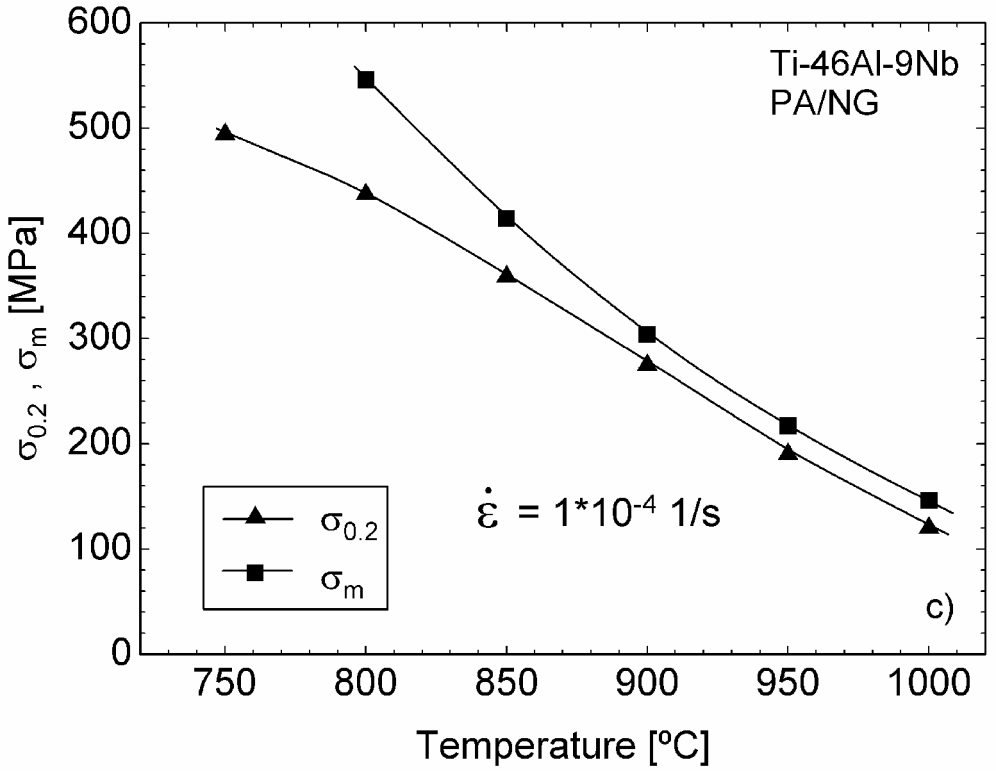
Ti-46Al-9Nb
PA/NG
$\sigma_{0.2}$, σ_m [MPa]
$\dot{\varepsilon}$ = 1*10^{-4} 1/s
$\sigma_{0.2}$
σ_m
c)
Temperature [ºC]
0
100
200
300
400
500
600
750
800
850
900
950
1000

Figure 4c

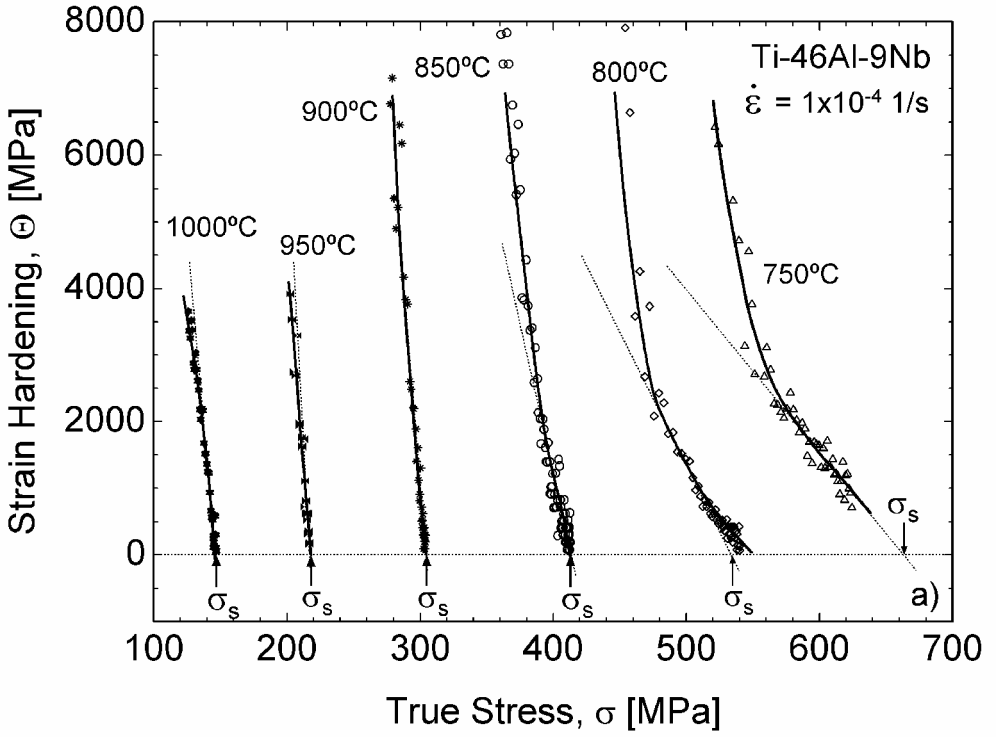

Figure 5a

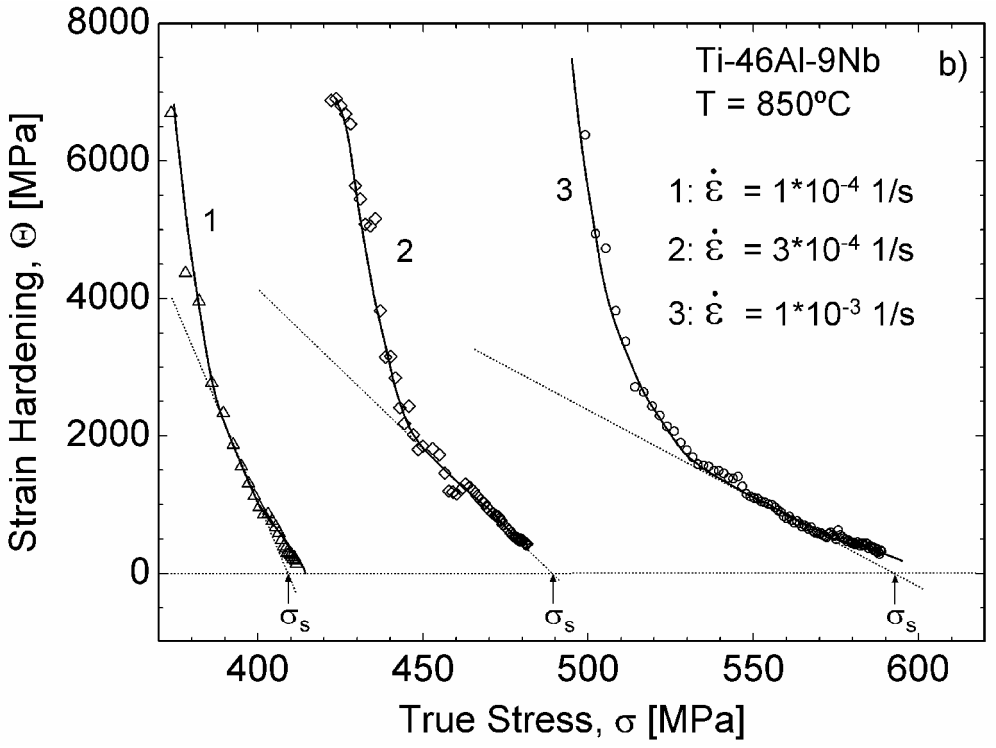

Figure 5b

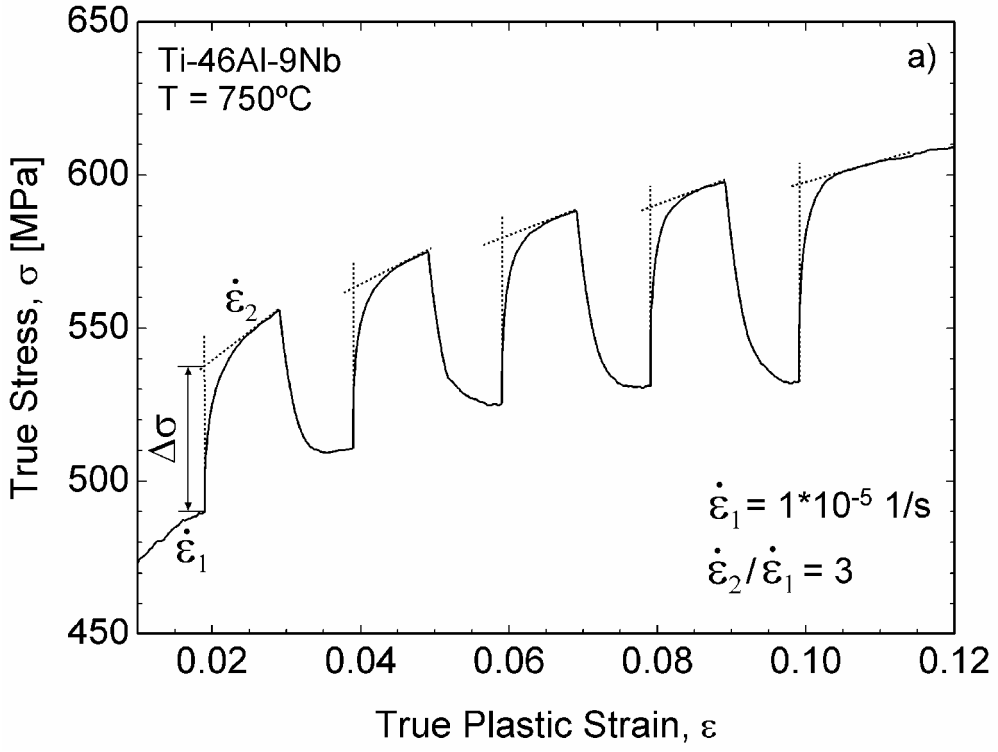

Figure 6a

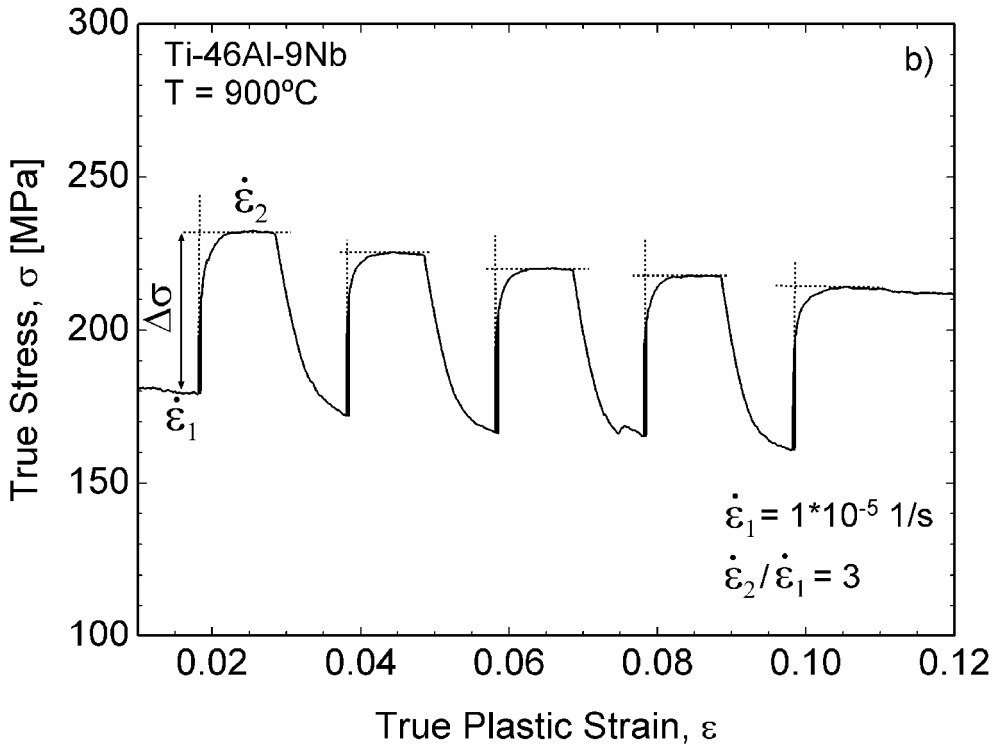

Figure 6b

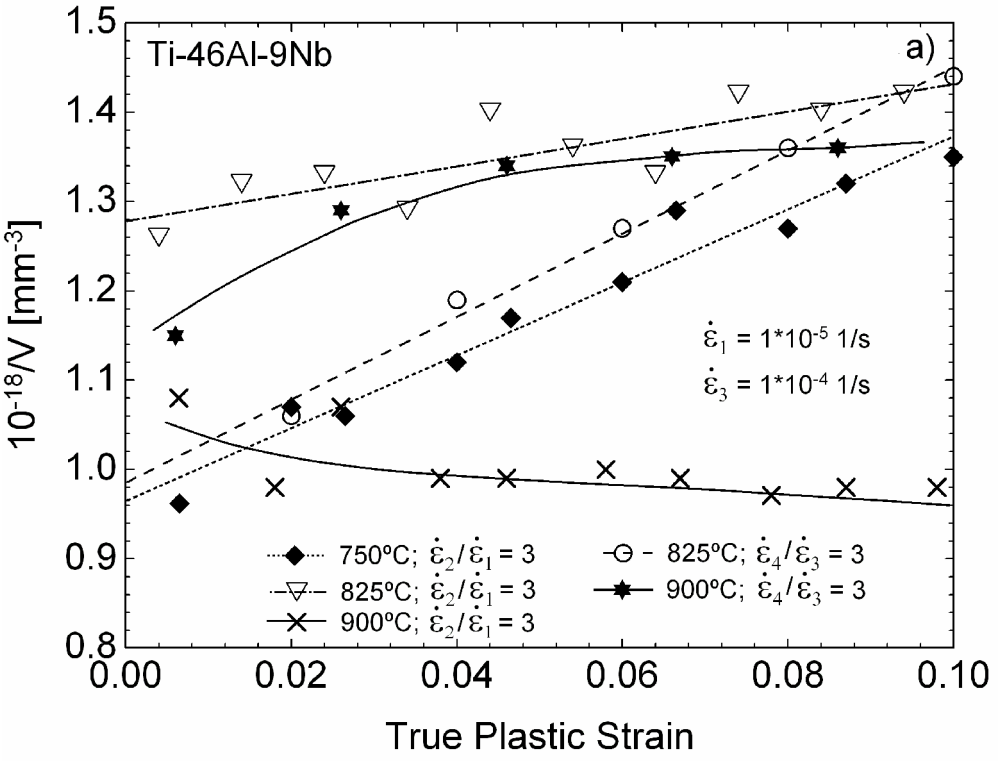

Figure 7a

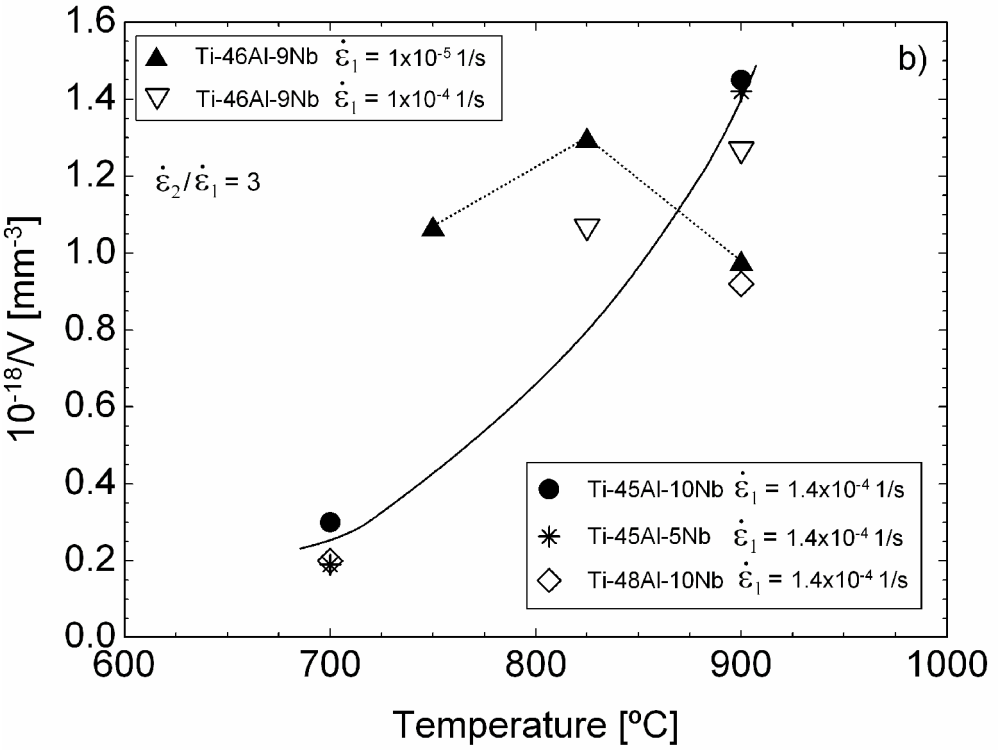

Figure 7b

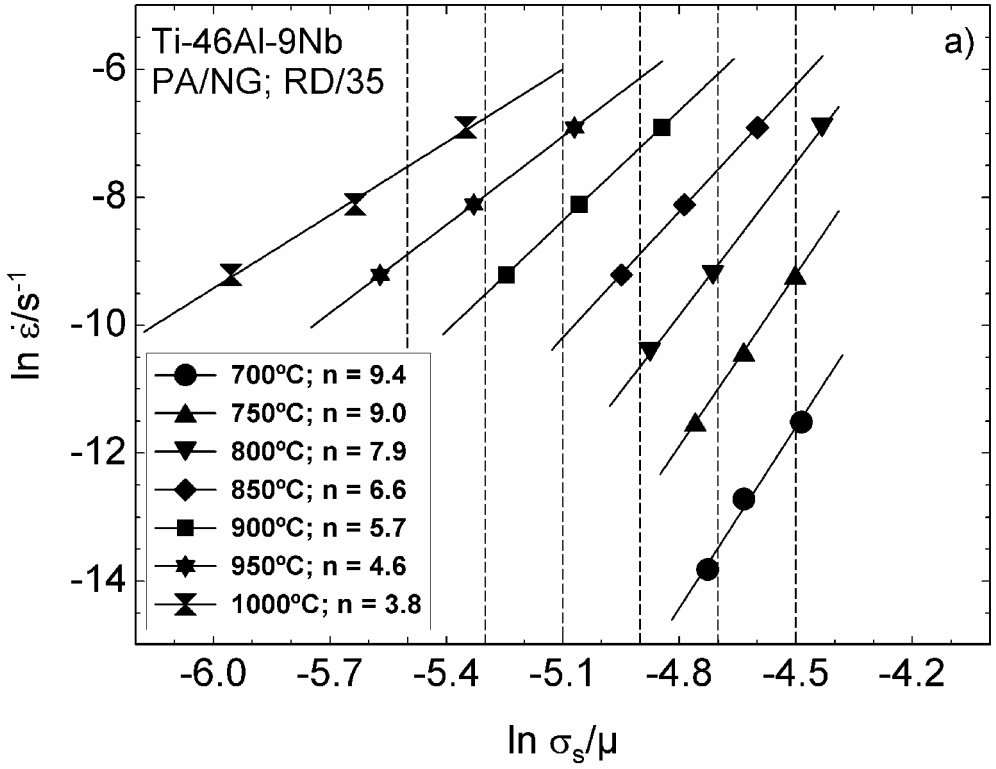

Figure 8a

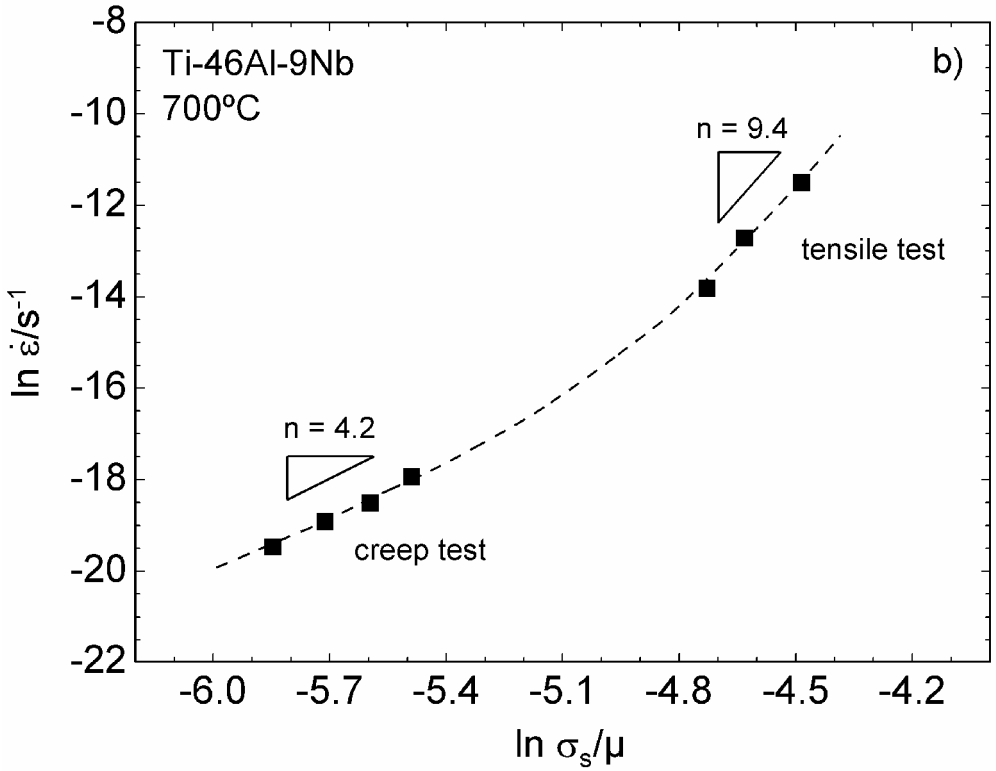

Figure 8b

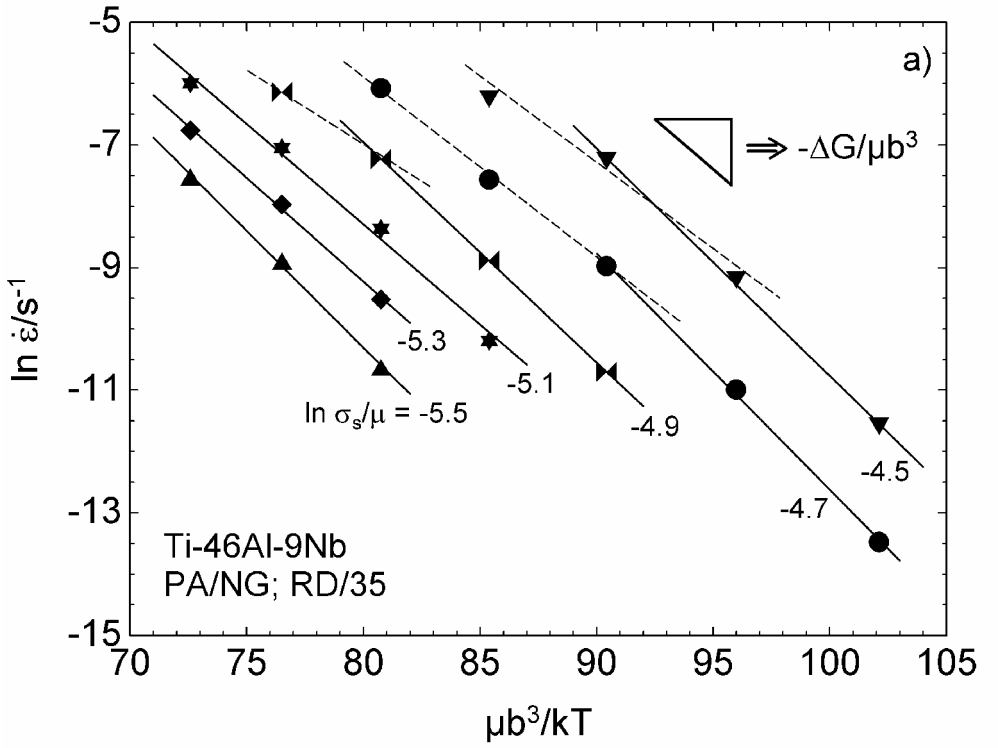

Figure 9a

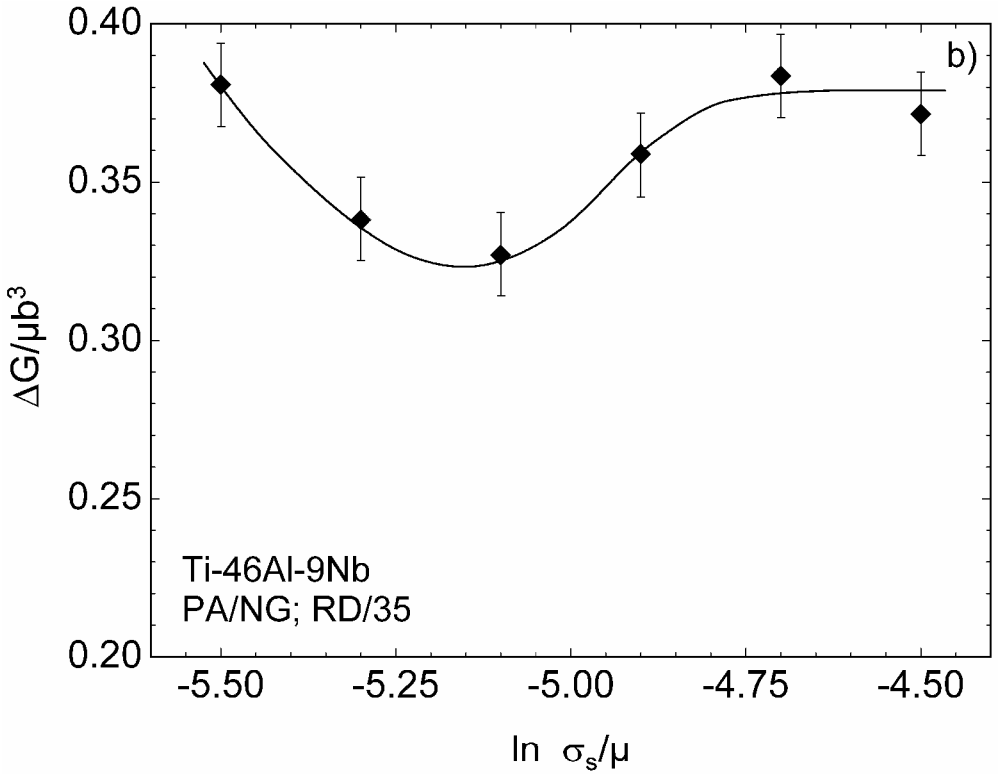

Figure 9b

*** Response to Reviewers**

Dear Dr. Sauthoff,

We like to thank both reviewers for their comments and suggestions on our paper (No.: INTERMETALLICS-D-07-00406) „Characteristics of the tensile flow behaviour of Ti-46Al-9Nb sheet-material - Analysis of thermally activated processes of plastic deformation“ by S. Bystrzanowski, A. Bartels, H. Clemens, R. Gerling.

For easier reading we copied the original comments and reply to them one by one. In the revised manuscript all changes are marked in yellow.

Comment from Reviewer #1:

It is strongly recommended to publish this well elaborated article based on extended experimental testing, detailed analysis of experimental data and very good discussion of achieved results. However, microstructural evidence of described deformation mechanisms is missing. It is mentioned that such analysis will be included in a separate article, which may be published soon.

Such an analysis of the microstructure evolution was planed but is not available at the moment. We deleted the following sentence with the link to “part 2 of this study” on page 9: *“The evidence of the slip bands was proven by microstructural observations is shown in part 2 of this study.”*

On page 16 we changed the sentence: “*These structural processes have been investigated by means of SEM and X-ray examinations and are discussed in the second part of this work”* into *“These structural processes have been investigated by means of SEM and X-ray examinations [33].”* The included reference [33] describes these investigations after creep. The old reference [33] has now the number [34].

Comment from Reviewer #2:

Only one small typing error could be detected, p.9, line 7: „...observations and is shown ..." (insert: „and").

This sentence was deleted (see above).

A small comment concerns the extrapolations to sigma_s in Fig. 5 a,b, which sometimes seems to be slightly arbitrary and may have been done with respect to optimizing the results in Fig. 8 a. Therefore, it would be helpful to include error bars to the values in

Fig. 8 a (and if possible also in Fig. 8 b), at least for some examples. Similarly, error bars should be provided for the DeltaG values in Fig. 9 b, so that the reader can judge the significance of the shown variation of DeltaG.

We followed the suggestion of the reviewer and include error bars to figure 9b. In figures 8a and 8b the possible error is not greater than the symbol size. We include on page 14 the sentences:

The experimental error in ln σ_s/μ results from the linear extrapolation for the determination of σ_s (Fig. 5). The error ranges around the size of the symbols and, therefore, is not shown in Fig. 8a.

And on page 15:

The error bars in Fig. 9b reflect the uncertainty in $\Delta G/\mu b^3$ due to the experimental errors in σ_s.

We marked the changes by high-lighting in yellow.

Yours sincerely,

Arno Bartels

On-behalf of all co-authors